Statistical characterization of the interchange-instability spectrum of a separable ideal-magnetohydrodynamic model system

R. L. Dewar,[1,2,*] T. Tatsuno,[3,2] Z. Yoshida,[2] C. Nührenberg,[4] and B. F. McMillan[1]
[1]*Department of Theoretical Physics and Plasma Research Laboratory, Research School of Physical Sciences and Engineering, The Australian National University, ACT 0200, Australia*
[2]*Graduate School of Frontier Sciences, University of Tokyo, 5-1-5 Kashiwanoha, Kashiwa-shi, Chiba 277-8651, Japan*
[3]*Institute for Research in Electronics and Applied Physics, University of Maryland, College Park, Maryland 20742-3511, USA*
[4]*Max-Planck-Institut für Plasma Physik, Teilinstitut Greifswald, D-17491, Germany*
(Received 3 May 2004; published 27 December 2004)

A Suydam-unstable circular cylinder of plasma with periodic boundary conditions in the axial direction is studied within the approximation of linearized ideal magnetohydrodynamics (MHD). The normal mode equations are completely separable, so both the toroidal Fourier harmonic index n and the poloidal index m are good quantum numbers. The full spectrum of eigenvalues in the range $1 \leqslant m \leqslant m_{\max}$ is analyzed quantitatively, using asymptotics for large m, numerics for all m, and graphics for qualitative understanding. The density of eigenvalues scales like $m_{\max}^2$ as $m_{\max} \to \infty$. Because finite-m corrections scale as $1/m_{\max}^2$, their inclusion is essential in order to obtain the correct statistics for the distribution of eigenvalues. Near the largest growth rate, only a single radial eigenmode contributes to the spectrum, so the eigenvalues there depend only on m and n as in a two-dimensional system. However, unlike the generic separable two-dimensional system, the statistics of the ideal-MHD spectrum departs somewhat from the Poisson distribution, even for arbitrarily large $m_{\max}$. This departure from Poissonian statistics may be understood qualitatively from the nature of the distribution of rational numbers in the rotational transform profile.

DOI: 10.1103/PhysRevE.70.066409 PACS number(s): 52.35.Bj, 05.45.Mt

I. INTRODUCTION

The general aim of this paper is to compare and contrast the spectrum of eigenvalues in typical integrable wave systems (e.g., waves in a rectangular cavity [1]) with the spectrum of instabilities in a cylindrical plasma within the ideal magnetohydrodynamics (MHD) approximation. This is a first step in understanding the spectral problem in the complex three-dimensional geometry of the class of magnetic confinement fusion experiments known as stellarators [2].

In ideal MHD the spectrum of the frequencies, ω, of normal modes of displacements about a toroidal equilibrium is difficult to characterize mathematically because the linearized force operator is not compact [3]. In addition to a point (discrete) spectrum of unstable modes ($\omega^2 < 0$), there are the Alfvén and slow-magnetosonic continuous spectra on the stable side of the origin ($\omega^2 > 0$) and the possibility of dense sets of accumulation points on the unstable side. In mathematical spectral theory, the stable continua and unstable accumulation "continua" [4] are characterized [5] as belonging to the *essential spectrum*. (For a self-adjoint operator L, the essential spectrum is the set of λ values for which the range of $L-\lambda$ is not a closed set and/or the dimensionality of the null space of $L-\lambda$ is infinite.)

There is experimental evidence that ideal MHD is relevant in interpreting experimental results [6,7], but perhaps the greatest virtue of ideal MHD in fusion plasma physics is its mathematical tractability as a first-cut model for assessing the stability of proposed fusion-relevant experiments with complicated geometries in the predesign phase.

For this purpose, a substantial investment in effort has been expended on developing numerical matrix eigenvalue programs, such as the three-dimensional TERPSICHORE [8] and CAS3D [9] codes. These solve the MHD wave equations for perturbations about static equilibria, so that the eigenvalue ω^2 is real due to the Hermiticity (self-adjointness [10]) of the linearized force and kinetic energy operators. They use finite-element or finite-difference methods to convert the infinite-dimensional PDE eigenvalue problem to an approximating finite-dimensional matrix problem. An alternative approach is to use local analysis using the ballooning representation and to attempt semiclassical quantization to estimate the global spectrum [11–13].

In order properly to verify the convergence of these codes in three-dimensional geometry, it is essential to understand the nature of the spectrum—if it is quantum-chaotic, then convergence of individual eigenvalues cannot be expected and a statistical description must be used [14–17].

This is perhaps of most importance in understanding the spectrum in three-dimensional magnetic confinement geometries, in particular the various stellarator experiments currently running or under construction. These devices are called three-dimensional because they possess no continuous geometrical symmetries, and thus there is no separation of variables to reduce the dimensionality of the eigenvalue problem. It has been shown [18] that the semiclassical limit (a Hamiltonian ray tracing problem) for ballooning instabilities in such geometries may be strongly chaotic because there are no ignorable coordinates in the ray Hamiltonian.

However, the present paper discusses the opposite limit, a system with a sufficient number of symmetries to make the

*Electronic address: robert.dewar@anu.edu.au

ray Hamiltonian integrable and the eigenvalue problem separable. The geometry is the circular cylinder, periodic in the z direction to make it topologically toroidal—we shall refer to the z direction as the toroidal direction and the azimuthal, θ direction as the poloidal direction. The study of this separable system will provide a baseline for comparison with the three-dimensional toroidal case in future work. The overall goal of the paper is to determine if the ideal-MHD spectrum falls within the same universality class as that of typical waves in separable geometries or, if not, what might cause it to differ.

Berry and Tabor [19] show that the distribution function $P(s)$ for the spacing of adjacent energy levels (suitably scaled) in a generic separable quantum system with more than one degree of freedom is $\exp(-s)$, as for a Poisson process with levels distributed at random. They also show that the spectrum of uncoupled quantum oscillators is nongeneric even when the frequency ratios are not commensurate, in which case $P(s)$ peaks about a nonzero value of s (as also occurs in nonintegrable, chaotic systems—the "level repulsion" effect). A more surprising departure from the Poisson distribution was found by Casati *et al.* [1] for waves in a rectangular box with irrational aspect ratio, but the departure was very small. Level spacing statistics are discussed also in the standard monographs on quantum chaos [14–17].

In contrast with quantum mechanics, where the continuous spectrum arises from the unboundedness of configuration space, the ideal-MHD essential spectrum arises from the unboundedness of Fourier space—there is no minimum wavelength. This is an unphysical artifact of the ideal MHD model because, in reality, low-frequency instabilities with $|\mathbf{k}_\perp|$ much greater than the ion Larmor radius, a_i, cannot exist (where $\mathbf{k}_\perp$ is the projection of the local wave vector into the plane perpendicular to the magnetic field $\mathbf{B}$). Indeed, ideal MHD breaks down in various ways at large $|\mathbf{k}_\perp|$, with dissipative and drift effects coming into play.

In this paper, we do not attempt to model finite-Larmor-radius stabilization, but instead simply restrict the poloidal mode spectrum to $m \leqslant m_{\max}$ and study the scaling of the spectrum at large $m_{\max}$. The nature of the dispersion relation is such that the toroidal mode numbers n relevant to the spectrum are also restricted. In a matrix eigenvalue code such as CAS3D or TERPSICHORE, our procedure corresponds to using an arbitrarily fine radial mesh but truncating the toroidal and poloidal basis set.

The eigenvalue equation for a reduced MHD model of a stellarator is presented in Sec. II. We study a plasma in which the Suydam criterion [20] for the stability of interchange modes is violated, so the number of unstable modes is infinite.

Section III is devoted to developing an understanding of the dependence (the *dispersion relation*) of the eigenvalues on the radial, poloidal, and toroidal mode numbers, l, m, and n, respectively. As m and n approach infinity, keeping $\mu \equiv n/m$ fixed, the growth-rate eigenvalues asymptote to a constant, the Suydam growth rate, depending only on μ and the radial mode number l. We use a combination of perturbation expansion in $1/m$ and numerical solution of the eigenvalue equation using a new transformation to Schrödinger form that is applicable over the whole range of m, from $O(1)$ to ∞. This generalizes the approach of Cheremhykh and Revenchuk [21], which was limited to the $m=\infty$ Suydam eigenvalue problem. We compare some of the asymptotic results in [21] with our numerical solutions. Our perturbation expansion shows that the correction to the Suydam limit goes as $1/m^2$. Contrary to usual experience [22], our numerical solutions show that the growth rates do not always approach the Suydam values from below as $m \to \infty$.

In Sec. IV, we examine the part of the spectrum involving the most unstable modes, which is essentially two-dimensional because only the lowest-order radial mode, $l=0$, contributes. We relate the considerable amount of structure observed in the spectrum to the Farey sequences of rational values of the rotational transform (winding number) of the equilibrium magnetic field. Low-order rationals have associated eigenvalue sequences giving a regular distribution of eigenvalues locally more like the spectrum of a one-dimensional system than a two-dimensional one.

In Sec. V, we derive the analog of the Weyl formula for the average density of states, including an asymptotic analysis of the large-l limit. In Sec. VI, we show level spacing distributions $P(s)$. Since we are interested in large m, we first try approximating the eigenvalues by their corresponding asymptotic Suydam limit. This gives a very singular distribution with a δ-function-like spike at the origin [23] due to the extremely degenerate nature of the spectrum in this approximation. By contrast, the distribution for the exact spectrum has no spike at the origin, showing that the small $1/m^2$ corrections break the degeneracy sufficiently to completely change the statistics.

We examine the statistics for the $l=0$ and $l=1$ spectra, both individually and combined (in the low-growth-rate region where they overlap). We have examined sufficiently large data sets to show convincingly that the statistical distributions are not Poissonian, though that of the combined $l=0$ and $l=1$ spectrum is closest. We also split the $l=0$ spectrum into two halves to remove overlap of spectra arising from different parts of the plasma. These split spectra exhibit a much more dramatic departure from Poisson statistics, showing that the ideal-MHD interchange spectrum is indeed nongeneric in the sense of Berry and Tabor [19].

II. CHOICE OF MODEL EIGENVALUE EQUATION

The grand context of this paper is the three-dimensional linearized ideal MHD problem—to solve, under appropriate boundary conditions, the equation of motion

$$\rho \partial_t^2 \boldsymbol{\xi} = \mathsf{F} \cdot \boldsymbol{\xi} \tag{1}$$

for small displacements $\boldsymbol{\xi}(\mathbf{r},t)$ of the MHD fluid about a static equilibrium state, where $\rho(\mathbf{r})$ is the equilibrium mass density, $\mathbf{r}$ is position, t is time, and F is a Hermitian linearized force operator [10] under the inner product $\int d^3x \boldsymbol{\xi}^* \cdot \mathsf{F} \cdot \boldsymbol{\xi}$ and suitable boundary conditions. (Superscript * denotes complex conjugation—we can take $\boldsymbol{\xi}$ to be complex because all the coefficients in F are real, so the real and imaginary parts of $\boldsymbol{\xi}$ obey the same equation.)

Most modern magnetic confinement fusion experiments, in particular tokamaks and stellarators, are toroidal. Though

not guaranteed for arbitrary three-dimensional systems, the equilibrium magnetic field $\mathbf{B}(\mathbf{r})$ is normally assumed to be *integrable* in the sense that all field lines lie on invariant tori (magnetic surfaces) nested about a single closed field line (the magnetic axis). Within each toroidal magnetic surface, a natural angular coordinate system is set up, with the poloidal angle θ increasing by 2π for each circuit around the short way and the toroidal angle ζ increasing by 2π for each circuit the long way. Each surface is characterized by a magnetic winding number, the *rotational transform* ι, being the average poloidal rotation of a field line per toroidal circuit, $\langle d\theta/d\zeta\rangle$, over an infinite number of circuits. (In tokamak physics the inverse, $q\equiv 1/\iota$, is normally used as the rotation number.)

In this paper, we study an effectively circular-cylindrical MHD equilibrium, using cylindrical coordinates such that the magnetic axis coincides with the z axis, made topologically toroidal by periodic boundary conditions. Thus z and the toroidal angle ζ are related through $\zeta\equiv z/R_0$, where R_0 is the major radius of the toroidal plasma being modeled by this cylinder. The poloidal angle θ is the usual geometric cylindrical angle and the distance r from the magnetic axis labels the magnetic surfaces (the equilibrium field being trivially integrable in this case). The plasma edge is at $r=a$.

In the cylinder there are two ignorable coordinates, θ and ζ, so the components of $\boldsymbol{\xi}$ are completely factorizable into products of functions of the independent variables separately. In particular, we write the r component as

$$r\xi_r = \exp(im\theta)\exp(-in\zeta)\varphi(r), \tag{2}$$

where the periodic boundary conditions quantize m and n to integers and we choose to work with the stream function $\varphi(r)\equiv r\xi_r(r)$.

Since the primary motivation of this paper is stellarator physics, we use the reduced MHD ordering for large-aspect stellarators [2,24], averaging over helical ripple to reduce to an equivalent cylindrical problem [25,26]. The universality class should be insensitive to the precise choice of model as long as it exhibits the behavior typical of MHD instabilities in a cylindrical plasma, specifically the existence of interchange instabilities and the occurrence of accumulation points at finite growth rates.

We nondimensionalize by measuring the radius r in units of the minor radius of the plasma column, a, and the time t in units of the poloidal Alfvén time $\tau_A=R_0\sqrt{\mu_0\rho}/B_0$, where B_0 is the toroidal magnetic field and μ_0 is the permeability of free space. Thus ω is in units of τ_A^{-1}. Defining $\lambda\equiv\omega^2$, we seek the spectrum of λ values satisfying the scalar equation

$$L\varphi = \lambda M\varphi \tag{3}$$

under the boundary conditions $\varphi(0)=0$ at the magnetic axis and $\varphi(1)=0$, appropriate to a perfectly conducting wall at the plasma edge. The operators L and M given below are Hermitian under the inner product defined, for arbitrary functions f and g satisfying the boundary conditions, by

$$\langle f,g\rangle \equiv \int_0^1 f^*(r)g(r)rdr. \tag{4}$$

The weight factor r in the inner product is a Jacobian factor coming from $d^3x=rdrd\theta dz$.

The operator L is given by

$$L \equiv -\frac{1}{r}\frac{d}{dr}(n-m\iota)^2 r\frac{d}{dr} + \frac{m^2}{r^2}\left[(n-m\iota)^2 - D_S + \frac{\ddot{\iota}}{m}(n-m\iota)\right], \tag{5}$$

where the Suydam stability parameter D_S is

$$D_S \equiv -\frac{\beta_0}{2\epsilon^2}p'(r)\Omega'(r), \tag{6}$$

with $\epsilon\equiv a/R_0\ll 1$ the inverse aspect ratio, $p(r)$ the plasma pressure normalized to unity at $r=0$, $\beta_0\equiv 2\mu_0 p_0/B_0^2$ the ratio of plasma pressure to magnetic pressure at the magnetic axis, and Ω' the average field line curvature. Here

$$\Omega \equiv \epsilon^2 N\left(r^2\iota + 2\int r\iota dr\right), \tag{7}$$

where the rotational transform is produced by helical current windings making $N\gg 1$ turns as ζ goes from 0 to 2π, $\Omega'(r)$ giving the averaged field-line curvature. (Note that ϵ cancels out in D_S.) We use the notation $\dot{f}\equiv rf'(r)$ for an arbitrary function f, so $\dot{\iota}\equiv rd\iota/dr$ is a measure of the magnetic shear and $\ddot{\iota}$ measures the variation of the shear with radius. The term Ω is a measure of the "magnetic hill" [2] that allows pressure energy to be released by interchanging field lines, thus driving the interchange instability.

The operator arising from the inertial term in Eq. (1),

$$M \equiv -\nabla_\perp^2 = -\frac{1}{r}\frac{d}{dr}r\frac{d}{dr} + \frac{m^2}{r^2}, \tag{8}$$

is easily seen to be positive definite under the inner product Eq. (4).

We observe some differences between Eq. (3) and the standard quantum-mechanical eigenvalue problem $H\psi=E\psi$. One is of course the physical interpretation of the eigenvalue—in quantum mechanics the eigenvalue $E\equiv\hbar\omega$ is linear in the frequency because the Schrödinger equation is first order in time, whereas our eigenvalue λ is quadratic in the frequency because it derives from a classical equation of motion.

Another difference is that Eq. (3) is a *generalized* eigenvalue equation because M is not the identity operator. This is one reason why it is necessary to treat the MHD spectrum explicitly rather than simply assume it is in the same universality class as standard quantum-mechanical systems.

Just as in ordinary eigenvalue problems, the eigenvalue spectrum for the generalized eigenvalue problem is real, and the eigenfunctions φ_i have a generalized orthogonality property

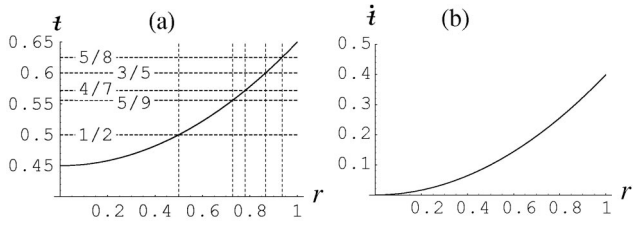

FIG. 1. (a) The rotational transform $\iota \equiv 1/q$, defined by Eq. (11), as a function of r in units of the minor radius; (b) the radial profile of the magnetic shear parameter $\dot{\iota} \equiv r\iota'(r)$. In (a), all distinct rational magnetic surfaces $\iota = \mu \equiv n/m$ are shown for m up to 10.

$$\langle \varphi_i, M\varphi_j \rangle = \delta_{i,j}, \tag{9}$$

where the normalization has been chosen to make the coefficient of the Kronecker δ unity. Here i and j denote members of the set $\{l,m,n\}$, where l is the radial node number and the poloidal and toroidal mode numbers m and n, respectively, are defined in Eq. (2). The negative part of the spectrum, $\lambda = -\gamma^2 < 0$, corresponds to instabilities growing exponentially with growth rate γ.

Equation (3) is very similar to the normal mode equation analyzed in the early work on the interchange growth rate in stellarators by Kulsrud [25]. However, unlike this and most other MHD studies, we are concerned not with finding the highest growth rate, but in characterizing the complete set of unstable eigenvalues.

III. INTERCHANGE SPECTRUM

In this section, we discuss the standard unregularized ideal MHD spectrum. It is well known that for $\lambda > 0$, the spectrum consists of the Alfvén continuum (the slow-magnetosonic continuum being removed in reduced MHD [27]). On the unstable side of the spectrum, $\lambda < 0$, it is also known that there is an infinity of eigenvalues provided the Suydam interchange instability criterion [20]

$$G \equiv \frac{D_S}{\iota^2} > \frac{1}{4} \tag{10}$$

is satisfied over some range of r in the interval (0, 1), but the details of the spectrum do not appear to have been published before.

A. Profiles

Interchange instabilities occur only for values of m and n such that $n - m\iota$ vanishes (or at least can be made very small [26]) and therefore it is important to know something about the function $\iota(r)$. The typical profile of $\iota(r)$ in a stellarator is monotonically increasing in the interval $[0,a]$ and we shall assume this to be the case here (though it is not always true in modern stellarators). For the numerical work in this paper, we use a parabolic profile

$$\iota = \iota_0 + \iota_2 r^2 \tag{11}$$

as illustrated in Fig. 1(a). In this and all subsequent plots, $\iota_0 = 0.45$, $\iota_0 = 0.2$.

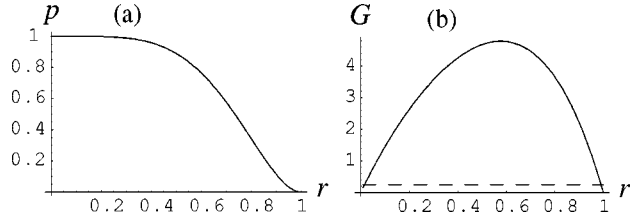

FIG. 2. (a) The nondimensional pressure profile $p(r)$, Eq. (13), used in this paper and (b) the Suydam criterion parameter $G(r)$, defined in Eq. (10) (solid line), and the instability threshold 1/4 (dashed line), showing nearly all the plasma is interchange unstable.

Given a rational fraction $\mu = n_\mu/m_\mu$ in the interval $[\iota(0), \iota(a)]$ (where n_μ and m_μ are mutually prime), there is a unique radius r_μ such that $\iota(r_\mu) = \mu$. Any pair of integers $(m,n)_{\mu,\nu} \equiv (\nu m_\mu, \nu n_\mu)$, $\nu = 1,2,3,\ldots$ satisfies the resonance condition

$$n_{\mu,\nu} - m_{\mu,\nu}\iota(r_\mu) = 0. \tag{12}$$

For example, the set of rationals with $1 < m \leqslant 10$ in the interval of ι shown in Fig. 1(a) is $\{\mu\} = \{1/2, 5/9, 4/7, 3/5, 5/8\}$, as shown in the figure.

To understand the global spectrum, we also need to know something about the pressure profile. In this paper, we use a broad pressure profile that is sufficiently flat near the magnetic axis that the Suydam instability parameter G defined in Eq. (10) goes to zero at the magnetic axis, and for which p' vanishes at the plasma edge

$$p(r) = 1 - 6r^5 + 5r^6. \tag{13}$$

(Recall from Sec. II that p is in units of the pressure at the magnetic axis.) This profile is shown in Fig. 2(a) and the resulting G profile in Fig. 2(b).

B. High *m* and *n*

In this subsection, we choose a particular rational surface r_μ and restrict attention to pairs (m,n) from the set $\{(m,n)_{\mu,\nu} | \nu = 1,2,3,\ldots\}$ satisfying the condition Eq. (12).

Defining a scaled radial variable $x \equiv m(r - r_\mu)/r_\mu$, we expand all quantities in inverse powers of m,

$$L \equiv \frac{m^2}{r_\mu^2}(L^{(0)} + m^{-1}L^{(1)} + m^{-2}L^{(2)} + \cdots),$$

$$M \equiv \frac{m^2}{r_\mu^2}(M^{(0)} + m^{-1}M^{(1)} + m^{-2}M^{(2)} + \cdots). \tag{14}$$

Also, $\lambda = \lambda^{(0)} + m^{-1}\lambda^{(1)} + m^{-2}\lambda^{(2)}$, and similarly for φ. The detailed expressions are given in Appendix A.

We then solve Eq. (3) by equating the LHS to zero order by order. At $O(m^0)$, as found by Kulsrud [25], we have the generalized eigenvalue equation

$$\mathcal{L}^{(0)}\varphi^{(0)} = 0, \tag{15}$$

where

$$\mathcal{L}^{(0)} \equiv L^{(0)} - \lambda^{(0)} M^{(0)} = -\frac{d}{dx}(\dot{\iota}^2 x^2 - \lambda^{(0)})\frac{d}{dx} + \dot{\iota}^2 x^2 - \lambda^{(0)} - D_S \tag{16}$$

with $\dot{\iota}$ and D_S evaluated at r_μ. For $\lambda^{(0)} < 0$, Eq. (15) can be solved to give a square-integrable eigenfunction under the boundary conditions $\varphi^{(0)} \to 0$ as $r \to \pm\infty$ when $\lambda^{(0)}$ is one of the eigenvalues $\lambda_{\mu,l}$, $l = 0, 1, 2, \ldots$, denoting the number of radial nodes of the eigenfunction $\varphi^{(0)} = \varphi_{\mu,l}$. Note that $\lambda_{\mu,l}$ depends only on $\mu = n/m$ and is otherwise independent of the magnitude of m and n. We assume that the $\varphi_{\mu,l}(r)$, when combined with the continuum generalized eigenfunctions for $\lambda^{(0)} > 0$, form a complete set.

1. Suydam approximation

The leading term in the expansion of the eigenvalue in $1/m$ gives the growth rate in the limit $m \to \infty$, known as the *Suydam approximation*. Restricting attention to unstable modes, so that $\gamma \equiv (-\lambda)^{1/2}$ is real, we transform Eq. (15) to the Schrödinger form [21]

$$\frac{d^2\psi}{d\eta^2} + Q(\eta)\psi = 0, \tag{17}$$

where

$$Q = Q_0(\eta|\gamma,\mu) \equiv G - \tfrac{1}{4} - \tfrac{1}{4}\,\mathrm{sech}^2\,\eta - \Gamma^2 \cosh^2\,\eta, \tag{18}$$

with $G \equiv G(r_\mu)$ defined as in Eq. (10), $\Gamma \equiv \gamma/\dot{\iota}(r_\mu)$, η defined through $x \equiv \gamma \sinh \eta/\dot{\iota}(r_\mu)$, and $\psi \equiv (\cosh \eta)^{1/2}\varphi(x)$. [In Ref. [21], Eq. (18) is derived from the Fourier transform of Eq. (15), but we can also use the real-space version as the equation shares with the quantum oscillator the remarkable property of having the same general form in both Fourier space and real space.]

Cheremhykh and Revenchuk [21] (CR) have made an extensive study of the eigenvalues of Eq. (17) using the semiclassical quantization condition

$$\oint Q_0(\eta)^{1/2} d\eta = (2l+1)\pi, \tag{19}$$

which follows from the WKB ansatz $\psi = A(\eta)\exp \pm i \int Q_0^{1/2} d\eta$. CR derive several approximations, useful in appropriate limits, improving on the earlier result of Kulsrud [25]. In this paper, we use two of their results to compare with numerical solutions of Eq. (17). The first is Eq. (4.5) of [21],

$$\Gamma \approx \frac{4\sigma}{e}\exp\left[-\frac{\left(l+\frac{1}{2}\right)\pi}{2\sigma} - \frac{1}{4\sigma^2}\right], \tag{20}$$

which [combining the criteria given in CR's Eqs. (4.4) and (4.12)] is applicable when $\sigma \equiv (G - 1/4)^{1/2} \gg 1/2$. The second CR result we use is their Eq. (4.7),

$$\Gamma^2 \approx \frac{G - (2l+1)G^{1/2}}{1 + (4G)^{-1}}, \tag{21}$$

applicable when $G \gtrsim \Gamma^2 \gg 1$.

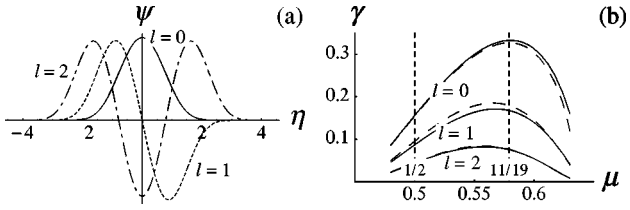

FIG. 3. (a) $m = \infty$ eigenfunctions for the $l = 0$ (solid line), $l = 1$ (short dashes), and $l = 2$ (short and long dashes) modes at $\mu = 1/2$, arbitrary normalization. (b) Growth rates γ (in units of the inverse poloidal Alfvén time) vs resonant $\dot{\iota} \equiv \mu$. Dashed lines show approximations Eq. (21) (for $l = 0$) and Eq. (20) (for $l = 1$ and 2).

As is seen from Fig. 3, Eq. (21) gives a remarkably good approximation to the growth rate of the most unstable radial eigenmode, $l = 0$, and Eq. (20) gives a good approximation for the higher-l modes (the semiclassical quantization being strictly justifiable only for large l). The growth-rate maxima for each l occur close to the maximum of G (and hence Γ), but not exactly owing to the $\dot{\iota}$ factor in the definition $\Gamma \equiv \gamma/\dot{\iota}(r_\mu)$.

From Eq. (21) we see that, provided the Suydam criterion $G > 1/4$ is satisfied, there is an infinity of growth rate eigenvalues accumulating exponentially toward the origin from above (so the λ values accumulate from below) in the limit $l \to \infty$.

Perhaps less widely appreciated (because m and n are normally taken to be fixed) is the fact that there is also a point of accumulation of the eigenvalues of Eq. (3) at each $\lambda_{\mu,l}$ as $m_{\max} \to \infty$ with l fixed. To break the degeneracy of $\lambda^{(0)}$, we must proceed further with the expansion in $1/m$.

2. $1/m^2$ corrections

Proceeding with the expansion Eq. (14), the calculation goes through much as in standard time-independent quantum perturbation theory [28], e.g..

The lowest-order eigenvalues and eigenfunctions are, as found in Sec. III B, $\lambda^{(0)} = \lambda_{\mu,l}$ and $\varphi^{(0)} = \varphi_{\mu,l}(x)$, respectively. The $O(1/m)$ correction, $\lambda^{(1)}$, vanishes identically from parity considerations—$\varphi_{\mu,l}(x)$ is either an even or odd function so its contribution to the matrix elements of $L^{(1)}$ and $M^{(1)}$ between $\varphi^{(0)}$ and $\varphi^{(0)}$ is even. On the other hand, $L^{(1)}$ and $M^{(1)}$ are odd, so $\lambda^{(1)} \equiv 0$. (This contrasts with the finite-aspect-ratio toroidal case where toroidal coupling of Fourier harmonics of different m to form ballooning modes leads to a nonvanishing $1/n$ correction [29,30].)

The first nonvanishing correction term is thus

$$\lambda^{(2)} = \langle \mu, l|\mathcal{L}^{(2)}|\mu, l\rangle - \sum_{l' \neq l} \frac{\langle \mu, l|\mathcal{L}^{(1)}|\mu, l'\rangle\langle \mu, l'|\mathcal{L}^{(1)}|\mu, l\rangle}{\lambda_{\mu,l'} - \lambda_{\mu,l}}, \tag{22}$$

where the sum over l' is taken to include an integration over the continuum. The operators $\mathcal{L}^{(i)} \equiv L^{(i)} - \lambda_{\mu,l} M^{(i)}$ are the higher-order generalizations of $\mathcal{L}^{(0)}$, defined by Eq. (16). The $m = \infty$ matrix elements of any operator $\mathcal{F}$ are defined by

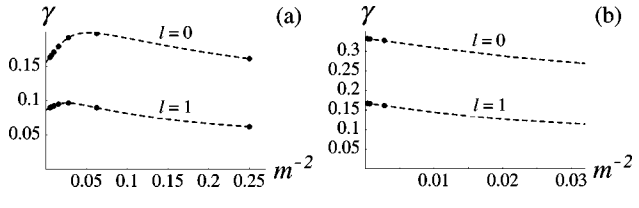

FIG. 4. Nondimensional growth rates $\gamma_{l,m,n} \equiv (-\lambda_{l,m,n})^{1/2}$ vs m^{-2} for $l=0$ and 1, found by numerical solution of Eq. (3) (Sec. III C): (a) $n/m=1/2$ $(m=2,4,6,\ldots)$ and (b) $n/m=11/19$ $(m=19,38,57,\ldots)$. At high m, the dependence becomes linear, in qualitative agreement with Sec. III B 2.

$$\langle \mu, l' | \mathcal{F} | \mu, l'' \rangle \equiv \int_{-\infty}^{\infty} \varphi^{*}_{\mu,l'}(x) \mathcal{F} \varphi_{\mu,l''}(x) dx, \tag{23}$$

with the eigenfunctions $\varphi_{\mu,l}(x)$ being normalized so that $\langle \mu, l | M^{(0)} | \mu, l \rangle = 1$. Note that, with the operators L and M defined as in Eqs. (5) and (8), $\mathcal{L}^{(i)}$ is Hermitian under the inner product used in Eq. (23) only for $i=0$. However, it can be made Hermitian at arbitrary order by the redefinitions $L \mapsto rL$ and $M \mapsto rM$, which puts the eigenvalue equation into Sturm-Liouville form.

As in quantum mechanics [28] e.g., if $\mathcal{L}^{(1)}$ is Hermitian the contribution of the second term on the right-hand side of Eq. (22) is always negative for the lowest eigenvalue, $\lambda_0^{(0)}$, because $\lambda_{l'}^{(0)} - \lambda_l^{(0)} > 0$. However, in ideal MHD a positive contribution from the first term usually dominates and the infinite-m mode is most unstable [22]. As seen in Fig. 4, this is not always the case: $\lambda_{l=0}^{(2)}$ is negative for $\mu=1/2$ but positive for $\mu=11/19=0.578\,947\ldots$.

The latter value of μ is very close to the value giving the global maximum Suydam growth rate (see Fig. 3). Thus, in the special case studied here and in accordance with conventional wisdom, the *global* maximum interchange growth rate occurs at $m=\infty$. Both these results are intuitively reasonable—the eigenfunctions become increasingly localized as $m \to \infty$, so the highest growth rate is obtained by localizing in the "most unstable" region of the plasma, where $\iota \approx 11/19$. On the other hand, modes which localize in "less unstable" regions as $m \to \infty$ can achieve a higher growth rate at finite values of m because their more extended finite-m eigenfunctions overlap the more unstable region and tap into the free energy from the pressure gradient in this region.

Since the eigenvalues approach $\lambda_{\mu,l}$ as $1/m^2$, there is an infinity of modes in the neighborhood of each $\lambda_{\mu,l}$ in the limit $m_{\max} \to \infty$. That is, they are finite-growth-rate accumulation points of the complete spectrum. Because the rationals μ are dense on the interval $(\iota(r_1), \iota(r_2))$, where (r_1, r_2) is the region in which the Suydam instability criterion is satisfied, and because $\lambda_{\mu,l}$ in general depends continuously on μ, the accumulation points $\lambda_{\mu,l}$ fill the interval $(-\gamma^2_{\max}, 0)$ densely. This is the part of the unstable spectrum called the "accumulation continuum" by Spies and Tataronis [4], though "accumulation essential spectrum" might be better terminology mathematically.

C. Finite *m* and *n*

In order to calculate arbitrarily high- or low-m eigenfunctions, we generalize the transformation in Sec. III B 1 by the change of variable from r to a new independent variable η such that

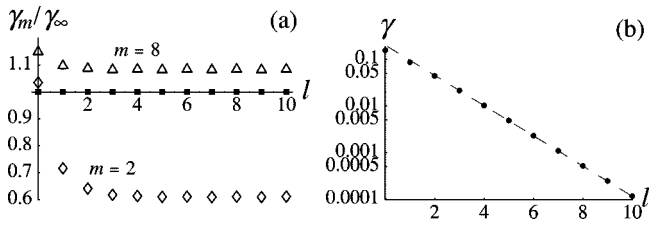

FIG. 5. Nondimensional growth rates vs radial node number l: (a) found by numerical solution of Eq. (3) (Sec. III C) for $(m,n)=(2,1)$ (diamonds) and (8, 4) (triangles), normalized to the $\mu=1/2$, infinite-m results (filled boxes); (b) $\mu=1/2$, infinite-m results (points) and asymptotic result Eq. (20) (dashed line).

$$m\iota(r) - n \equiv \gamma \sinh \eta, \tag{24}$$

and a new dependent variable $\psi(\eta)$ such that

$$\varphi \equiv (\dot{\iota} \cosh \eta)^{-1/2} \psi(\eta), \tag{25}$$

so that Eq. (3) becomes the Schrödinger equation (17), but with Q_0 replaced by

$$Q \equiv G(\eta) - \frac{1}{4} - \frac{\mathrm{sech}^2 \eta}{4} - \frac{\gamma^2}{\dot{\iota}^2} \cosh^2 \eta + \frac{\tanh \eta}{2\dot{\iota}} \frac{d\dot{\iota}}{d\eta} - \frac{1}{2\dot{\iota}} \frac{d^2\dot{\iota}}{d\eta^2} + \frac{1}{4\dot{\iota}^2} \left(\frac{d\dot{\iota}}{d\eta} \right)^2, \tag{26}$$

where $\dot{\iota} \equiv r d\iota/dr$ is as defined in previous sections, but expressed in terms of η.

Differentiating Eq. (24), we find

$$\frac{dr}{d\eta} = \frac{\gamma \cosh \eta}{\dot{\iota}} \frac{r}{m}. \tag{27}$$

Thus, in the large-m limit, equilibrium parameters such as G and $\dot{\iota}$ are slowly varying functions of η, e.g., $d\dot{\iota}/d\eta = O(1/m)$ and $d^2\dot{\iota}/d\eta^2 = O(1/m^2)$. Comparing Eq. (26) with Eq. (18), we see that, to leading order in $1/m$, $Q=Q_0$ but with $\dot{\iota}$ now a slow variable rather than a strict constant.

With the simple form for ι, Eq. (11), assumed in this paper, Eq. (24) is easily inverted to give $r(\eta)$, and also a cancellation occurs between the terms $\dot{\iota}'(\eta)\tanh \eta/2\dot{\iota}$ and $\dot{\iota}''(\eta)/2\dot{\iota}$, so that the exact Q is not much more complicated than Q_0. The eigenvalues in Figs. 4 and 5 were computed by integrating Eq. (17) with Q_0 replaced by the exact Q and with the appropriate finite boundary conditions. Low-m results were checked against those from an untransformed shooting code. The dashed lines represent the results of scans through unquantized, noninteger values of m to show the smooth, but not necessarily monotone, functional dependence of γ on m

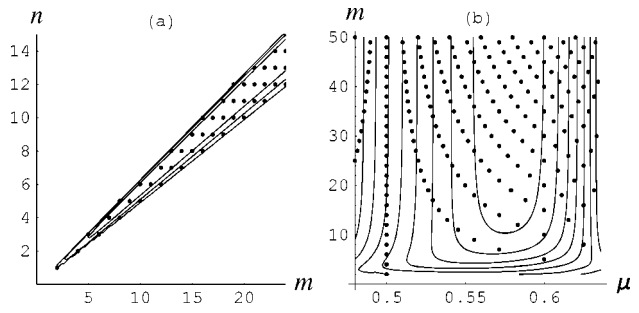

FIG. 6. (a) Lattice of quantum numbers on which the part of the spectrum between the "ground state" and the threshold for the entry of the $l=1$ mode is defined, and the unbounded contours of constant eigenvalue. (b) The same, in $\mu \equiv n/m$, m space.

IV. $l=0$ SPECTRUM

The most unstable modes are those with radial node number $l=0$. Thus we first consider the set $S_0 \equiv \{\lambda_{0,m,n} | 1 \leqslant m \leqslant m_{\max}, m\mu_{\min} < n < m\mu_{\max}\}$, where m and n are integers and $\mu_{\min}$ and $\mu_{\max}$ are chosen to give the desired range of γ. As we shall be rescaling the eigenvalues prior to statistical analysis, it makes no difference whether we work with the spectrum of growth rates γ or the eigenvalues $\lambda \equiv -\gamma^2$. However, the latter choice makes it clearer that the analog of the quantum-mechanical ground state is the most rapidly growing mode—denoting the maximum growth rate of the $l=0$ mode by γ_0, the minimum λ is $\lambda_0 = -\gamma_{\max}^2 = -\gamma_0^2$.

The spectrum is defined on the fanlike subset of the two-dimensional quantum-number lattice depicted in Fig. 6(a). Also shown are contours of constant γ (or λ), regarded as a continuous function of m and n, which are seen more clearly in Fig. 6(b). Here we see a striking contrast with more generic systems [19], where the constant-eigenvalue contours are segments of topological circles enclosing the origin. In the ideal-MHD case, the contours are topologically hyperbolic, with asymptotes radiating from the origin toward infinity.

An interesting representation of the $l=0$ spectrum is shown in Fig. 7. A great deal of structure can be discerned, determined by the number-theoretic properties of the interval of μ depicted. For instance, focusing on the low-order rational number 4/7, we define spectral subsets $S_0(N/M|4/7) \equiv \{\lambda_{0,m,n} | m = M+7k, n = N+4k, k = 0,1,2,\ldots,[(m_{\max}-N)/7]\}$, where $[x]$ denotes the largest integer $\leqslant x$.

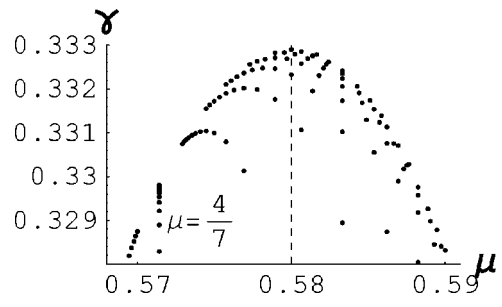

FIG. 7. Nondimensional growth-rate eigenvalues of $l=0$ modes near the maximum growth rate vs $\mu \equiv n/m$. The ensemble shown is for $m_{\max}=100$.

These spectral sequences all accumulate toward the same Suydam eigenvalue $\lambda_{4/7,0}$ as $m_{\max} \to \infty$ independently of the choice of M and N. However, the rapidity of this approach is sensitive to the choice of M/N. For instance, we see in Fig. 7 the most rapidly converging sequence, $S_0(4/7|4/7)$, as a set of points accumulating vertically from below toward the Suydam eigenvalue. Other sequences on either side of $S_0(4/7|4/7)$ approach the accumulation point obliquely and much more slowly—for $m_{\max}=100$ they visibly have some distance to go. The sequence immediately to the left of $S_0(4/7|4/7)$ is $S_0(1/2|4/7)$, while that to the right is $S_0(3/5|4/7)$, 1/2 and 3/5 being the immediate neighbors of 4/7 in the Farey sequence ([31], p. 300) of order 7 (the first order at which 4/7 appears), with the μ values corresponding to $S_0(1/2|4/7)$ and $S_0(3/5|4/7)$ providing the immediate neighbors of 4/7 in each higher-order Farey sequence.

In discussing the structure of the spectrum, it is useful to partition S_0 into two subsets, S_0^- and S_0^+, as the points are to the left or right, respectively, of the dashed vertical line shown in Fig. 7 passing through the point of maximum growth rate.

The sequences $S_0(1/2|4/7)$ and $S_0(3/5|4/7)$ accumulate toward $\lambda_{4/7,0}$, but slower $[O(1/m_{\max})]$ than does $S_0(4/7|4/7)$ $[O(1/m_{\max}^2)$, from Sec. III B 2]. Thus there is a gap containing $\lambda_{4/7,0}$ within which $S_0(4/7|4/7)$ contributes $O(m_{\max})$ points to S_0^-, while other sequences contribute at most a set of $O(1)$ points.

Within the gap, the spectrum S_0^- is essentially one-dimensional, being indexed by the single quantum number k. In the full spectrum, $S_0 = S_0^- \cup S_0^+$, $O(m_{\max})$ unrelated eigenvalues from S_0^+ appear in the gap, making the spectrum locally more random and two-dimensional.

V. WEYL FORMULA

As discussed in Sec. III B 2, the overall maximum growth rate for the $l=0$ and 1 modes (and, we assume, for all l) occurs at $m=\infty$. Thus the threshold value when a given mode l first starts contributing to the spectrum is at $\lambda = -\gamma_l^2$, where γ_l is the maximum over μ of $\gamma(\mu, l)$. We denote the corresponding value of μ by μ_l.

For fixed l and large $m_{\max}$, the number of eigenvalues $N_l(\mu)$ in an interval of n/m between μ_l and μ is asymptotically equal to the area in the m, n plane [see Fig. 6(a)] of the triangle bounded by the lines $n=\mu m$, $n=\mu_l m$, and $m=m_{\max}$. That is, $N_l(\mu) \sim \frac{1}{2}|\mu - \mu_l| m_{\max}^2$.

Since contours of constant λ (or γ) asymptote to lines of constant μ as $m \to \infty$, we can estimate the number of eigenvalues between two values of λ (or γ) by inverting the function $\lambda_{\mu,l}$ for μ and substituting this into the above expression for $N_l(\mu)$. The inverse is double-valued: $\mu = \mu_l^+(\lambda) > \mu_l$ and $\mu_l^-(\lambda) < \mu_l$. Then the number of eigenvalues between the ground state $\lambda_{\mu_0,l}$ and λ is approximately

$$\overline{N_l^{\pm}}(\lambda) \equiv \frac{1}{2}|\mu^{\pm}(\lambda) - \mu_0| m_{\max}^2. \tag{28}$$

The asymptotic dependence of the total spectrum $S \equiv S_0^- \cup S_0^+ \cup S_1^- \cup S_1^+ \cup \ldots$ is thus

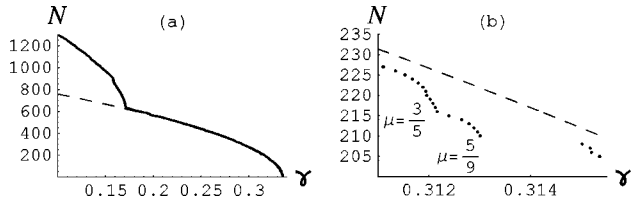

FIG. 8. (a) Eigenvalue sequence number $N(\gamma)$ for the combined spectral set $S_0 \cup S_1$ in the case $m_{\max}=100$. The Weyl formula for S_0, $\overline{N_0^-}(\gamma)+\overline{N_0^+}(\gamma)$, is shown as a dashed line. (b) Closeup of the region containing eigenvalues associated with $\mu=3/5$ and $\mu=5/9$.

$$\overline{N}(\lambda) \equiv \sum_{l=0}^{\infty} \sum_{\pm} \overline{N_l^{\pm}}(\lambda). \tag{29}$$

This is the analog of the Weyl formula [14, p. 258] for the integral of the smoothed spectral density ("density of states").

Approximating $\lambda_{\mu,l}=\lambda_l+\frac{1}{2}(\partial^2\lambda_{\mu_l,l}/\partial\mu_l^2)(\mu-\mu_l)^2$, we get $\mu_l^{\pm}(\lambda)=\mu_l\pm\sqrt{2}(\lambda-\lambda_l)^{1/2}/(\partial^2\lambda_{\mu_l,l}/\partial\mu_l^2)^{1/2}$. Thus there is a square-root singularity at each mode threshold.

A comparison between the Weyl formula for S_0 and the set of points $\{(\gamma_N,N)\}$, where N is the sequence number obtained by sorting the set of $l=0$ and $l=1$ growth-rate eigenvalues from largest to smallest, is shown in Fig. 8(a), showing excellent agreement above the threshold for S_1. The plotted points may also be regarded as the locations of the steps in the "staircase plot" of the piecewise-constant integrated density-of-states function $N(\gamma)$, but the scale in this plot is too coarse to resolve the staircase structure.

A finer-scale plot is shown in Fig. 8(b), in which significant deviations from the Weyl curve are seen in the microstructure. The range shown in Fig. 8(b) is unusual in that it contains *two* well-defined accumulation sequences in close proximity. These are associated with low-order values of μ occurring on either side of the growth-rate maximum near $\mu=11/19\approx 0.579$—the sequence associated with $\mu=5/9\approx 0.556$ is in S_0^- and the one associated with $\mu=3/5=0.6$ is in S_0^+. There are very few eigenvalues associated with high-order rational values of μ in the range shown and the two low-order sequences present are practically unmixed, either with each other or with eigenvalues associated with unrelated higher-order rational values of μ. [In fact there is only one such high-order mode in the region of the accumulation sequences, $\mu=51/92$, the closest approximant to $5/9$ in the set corresponding to $S_0(1/2|5/9)$, which causes the slight jump seen in the $\mu=3/5$ sequence.] Also, the wide gap containing no eigenvalues is because the intersection of the gaps associated with the two low-order rationals is nonempty.

The spectrum near the marginal stability point, $\gamma=0$, will involve the superposition of many branches of radial eigenvalue l. To estimate the asymptotic behavior of $N(\gamma)$ as $\gamma\to 0$, we use the approximate dispersion relation Eq. (20). Taking l to be large, we see from Eq. (20) that the Suydam growth rates $\gamma_l(\mu)$ are sharply peaked about the location of the maximum, μ_0, of $G(r_\mu)$, where $\sigma(\mu)\equiv(G-1/4)^{1/2}$ is also a maximum. Thus we can expand $\sigma(\mu)$ about μ_0,

$$\sigma(\mu)=\sigma_{\max}\left[1-\left(\frac{\mu-\mu_0}{\Delta\mu}\right)^2\right]+O[(\mu-\mu_0)^3], \tag{30}$$

where $(\Delta\mu)^2\equiv -2\sigma_{\max}/\sigma''(\mu_0)$. To leading order all other parameters are evaluated at the maximum point $\mu=\mu_0$. The quadratic correction to σ need only be retained in the term involving the expansion parameter l, so, to leading order,

$$\gamma_l \approx \gamma_0 \exp\left[-\frac{\pi l}{2\sigma(\mu)}\right], \tag{31}$$

where $\gamma_0\equiv 4\dot{\iota}(r_{\mu_0})(\sigma_{\max}/e)\exp(-\pi/4\sigma_{\max}-1/4\sigma_{\max}^2)$.

Solving for μ, we find

$$\mu_l^{\pm}(\gamma)=\mu_0\pm\Delta\mu\left[1-\frac{l}{l_{\max}(\gamma)}\right]^{1/2}, \tag{32}$$

where $l_{\max}(\gamma)\equiv(2/\pi)\sigma_{\max}\ln(\gamma_0/\gamma)$. Substituting Eq. (32) in Eq. (29) and approximating the sum over l by an integral, we find the leading-order asymptotic behavior of the number of eigenvalues to be

$$\overline{N}(\gamma)\sim\frac{4\Delta\mu}{3\pi}\sigma_{\max}m_{\max}^2\ln\frac{\gamma_0}{\gamma}, \tag{33}$$

which diverges logarithmically as $\gamma\to 0$.

VI. NEAREST-NEIGHBOR STATISTICS

Preparatory to the statistical analysis of eigenvalue spacing, it is standard practice to rescale, or *unfold*, the eigenvalues so as to make their average separation unity, thus making possible the comparison of different systems on the same footing.

We can unfold the spectra by using the Weyl formulas above, e.g., for $\lambda_i\in S_0^{\pm}$ we can define rescaled eigenvalues $E_i^{\pm}$ by

$$E_i^{\pm}\equiv\overline{N_0^{\pm}}(\lambda_i). \tag{34}$$

For the set $S_0=S_0^+\cup S_0^-$, we can unfold with the combined Weyl function, $\Sigma_{\pm}\overline{N_0^{\pm}}$. However, for practical purposes we have in this section used empirical least-square fits of $N(\gamma)$ to a linear superposition of the basis functions $(\gamma_{\max}-\gamma)^{1/2}$, $(\gamma_{\max}-\gamma)$, $(\gamma_{\max}-\gamma)^{3/2}$, which captures the square-root singularity but avoids having to invert $\gamma_{\mu,l}$.

When $m_{\max}$ is large, the great majority of eigenvalues $\lambda_{l,m,n}$ are very close to the corresponding $m=\infty$ eigenvalue with the same $\mu\equiv n/m$, $\lambda_{\mu,l}$. Thus one might suppose that the statistics of the spectrum are asymptotically the same as those of an ensemble $S_0^{\text{Suydam}}\equiv\{\lambda_{n/m,0}|1\leqslant m\leqslant m_{\max}, m\mu_{\min}<n<m\mu_{\max}\}$.

In Fig. 9(a), we show the distribution of nearest-neighbor unfolded eigenvalue spacings for S_0^{Suydam}, and in Fig. 9(b) that for the set S_0 with the correct finite-m eigenvalues. It is seen that the two distributions are radically different—even though low-order rational values of μ are rare and the distribution is coarse-grained, the high-m approximation induces sufficient extra degeneracy that the Suydam spectrum is dominated by a large, but spurious, δ-function-like spike at

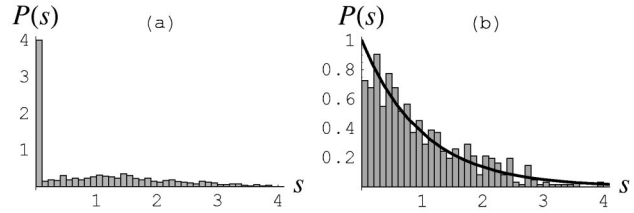

FIG. 9. (a) Nearest-neighbor eigenvalue spacing distribution for the approximate spectral set S_0^{Suydam} using $\mu_{\min}=0.5044$, $\mu_{\max}=0.6288$, $m_{\max}=100$ (625 eigenvalues). (b) The same, for the corresponding set of accurate eigenvalues S_0.

$s=0$. (The range of μ used in Fig. 9 corresponds to the range of $l=0$ growth rates above the maximum $l=1$ rate, in which S_0 is the only contributor to the spectrum.)

The reason why finite-m effects are so important, despite the smallness of the $O(1/m^2)$ corrections found in Sec. III B 2, is seen from the Weyl formula, Eq. (28), which shows that the *average* eigenvalue spacing in a set containing all values of n/m within the range of interest scales as $m_{\max}^{-2}$, which is the same order as the *smallest* $O(1/m^2)$ correction within a set containing only $n/m=\mathrm{const}$. Thus in the set of accurate eigenvalues S_0 there is a strong intermingling of eigenvalues with different n/m that does not occur in the approximate set S_0^{Suydam}.

This explains why the nearest-neighbor eigenvalue spacing distribution in Fig. 9(b) is much closer to the Poisson distribution $\exp(-s)$ obtained for a random distribution of numbers on the real line, and also predicted for generic separable systems [19], than that in Fig. 9(a). Nevertheless, the set of 625 eigenvalues used in Fig. 9(b) is too small to say convincingly that the distribution is or is not Poissonian, so we need to analyze larger data sets to determine how close to generic the ideal-MHD spectrum is.

A cutoff at $m_{\max}=1000$ gives a set S_0 containing about 62 254 eigenvalues in the range between the maximum $l=0$ growth rate and the maximum $l=1$ growth rate. [Note the approximately $m_{\max}^2$ scaling in the size of S_0, as predicted by the Weyl formula, Eq. (28).] In Fig. 10(a), we show the nearest-neighbor distribution for this set. Close examination of the region near the origin reveals no trace of the spike seen in Fig. 9(a), not even the tiny spike found by Casati *et al.* [1] for the spectrum of waves in an incommensurate rectangular box. However, it is clear that the statistics are not exactly Poissonian.

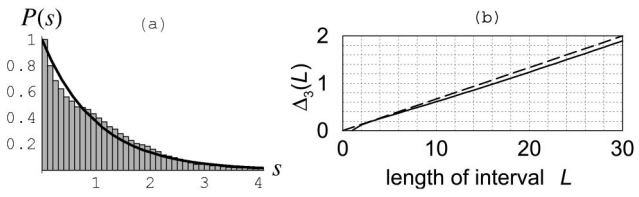

FIG. 10. (a) Nearest-neighbor eigenvalue spacing distribution for the spectral set S_0 using $\mu_{\min}=0.5044$, $\mu_{\max}=0.6288$, $m_{\max}=1000$ (62,254 eigenvalues). (b) The Dyson-Mehta spectral rigidity for this set (solid line) compared with that for the Poisson process (dashed line).

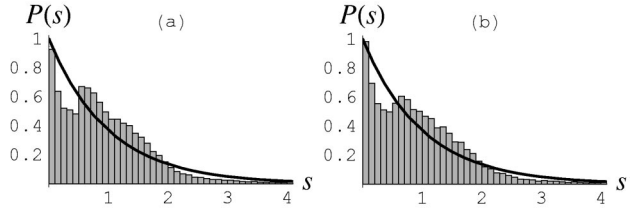

FIG. 11. (a) Nearest-neighbor eigenvalue spacing distribution for the spectral set S_0^- for $m_{\max}=1000$ (37 932 eigenvalues). (b) Nearest-neighbor eigenvalue spacing distribution for the spectral set S_0^+ (24 412 eigenvalues).

In Fig. 10(b), we show the Dyson-Mehta rigidity parameter $\Delta_3(L)$ [17, pp. 321-323], defined as the least-squares deviation of the unfolded eigenvalue staircase $N(E)$ from the best-fitting straight line in an interval of length L. Again, the behavior is similar to that for the completely random spectrum (Poisson process) in that Δ_3 increases linearly with L, but the slope is slightly less than the $1/15$ expected for the Poisson processs.

In order to understand the departure from Poisson statistics better, we show in Fig. 11 the spacing distribution for the corresponding sets S_0^- and S_0^+. The departure from Poisson statistics is now quite striking.

In Fig. 12(a), we show the spacing distribution for the $l=1$ spectrum, which is seen to be very much like the $l=0$ spectrum of Fig. 10(a) in its departure from the Poisson distribution. However, we might expect that mixing the $l=0$ with the $l=1$ spectrum will make the levels appear more "random" and Fig. 12(b) confirms that the level spacing distribution does indeed become more like the exponential expected for a Poisson process.

VII. CONCLUSION

We have demonstrated that the statistical nature of the ideal-MHD interchange spectrum deviates significantly from the random Poisson process of generic separable systems due to the number-theoretic structure of the eigenvalue distribution. The similarity between the two level-spacing distributions in Fig. 11, which correspond to two different parts of the rotational transform profile, suggests the possibility that there may nevertheless be some universality in the statistics. If so, we have found a new universality class.

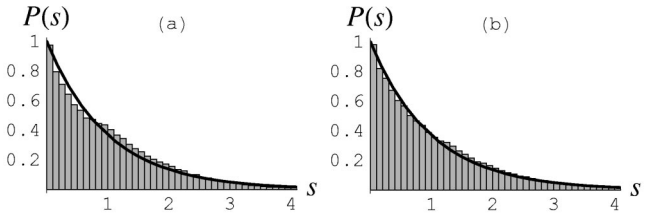

FIG. 12. (a) Nearest-neighbor eigenvalue spacing distribution for the first 72 500 eigenvalues of the $l=1$ spectral set S_1, $m_{\max}=1000$. (b) Nearest-neighbor eigenvalue spacing distribution for the mixed spectral set $S_0 \cup S_1$ over the same range of eigenvalues as in (a) (total of 95 000 eigenvalues).

The crude regularization used in this paper, simply restricting the poloidal mode numbers to $m \leqslant m_{\max}$, is not very physical but corresponds closely to what is done in the large three-dimensional eigenvalue codes CAS3D [9] and TERPSICHORE [8]. Thus, apart from fundamental mathematical interest, the primary motivation of this paper has been the numerical analysis of the three-dimensional ideal-MHD spectrum as produced by these codes. Preliminary results [23] on an interchange-unstable stellarator test case show spectra with eigenvalue separation statistics similar to those of strongly quantum chaotic systems. However, the results of the present paper indicate that some caution should be taken in interpreting ideal-MHD spectra in terms of conventional quantum chaos theory because of the radically different nature of the dispersion relation.

In subsequent work it will be important to examine the effect of the finite Larmor radius on the spectrum. However, this typically makes the problem non-Hermitian and less easy to compare with standard quantum chaos theory.

A preliminary attempt [23] to regularize MHD via a Hermiticity-preserving inverse-Larmor-radius cutoff in $|\mathbf{k}_\perp|$ found a much more Poissonian eigenvalue-spacing histogram for the $l=0$ spectrum than that found in the present paper. This suggests that finite-Larmor radius regularization is not only more physical than simple truncation in m and n, but also makes the spectrum more generic (provided the eigenvalues remain real).

ACKNOWLEDGMENTS

One of us (R.L.D.) acknowledges the support of the Australian Research Council and useful discussions with H. Friedrich, R. Mennicken, H. Schomerus, G. Spies, J. Wiersig, and N. Witte on spectral and quantum chaos issues forming the background of this paper.

APPENDIX A: $1/m^2$ CORRECTIONS

The coefficients of the expansion Eq. (14) are found by Taylor expansion of the geometric and equilibrium quantities in Eq. (5),

$$L^{(0)} = -\frac{d}{dx}\dot{\iota}^2 x^2 \frac{d}{dx} + \dot{\iota}^2 x^2 - D_S,$$

$$L^{(1)} = x\frac{d}{dx}\dot{\iota}^2 x^2 \frac{d}{dx} - \frac{d}{dx}\dddot{\iota}\iota x^3 \frac{d}{dx} + \dot{\iota}(\ddot{\iota} - 3\dot{\iota})x^3 + (2D_S - \dot{D}_S - \dddot{\iota}\iota)x,$$

$$L^{(2)} = -x^2\frac{d}{dx}\dot{\iota}^2 x^2 \frac{d}{dx} + x\frac{d}{dx}\dddot{\iota}\iota x^3 \frac{d}{dx} + \frac{d}{dx}x^4 \times\left(\frac{\dot{\iota}^2}{12} - \frac{\ddot{\iota}^2}{4} + \frac{\dddot{\iota}\iota}{2} - \frac{\ddddot{\iota}\iota}{3}\right)\frac{d}{dx} + \frac{x^2}{2} \times(5\dddot{\iota}\iota - 2\ddddot{\iota}\iota - \ddot{\iota}^2 - 6D_S + 5\dot{D}_S - \ddot{D}_S) + x^4 \times\left(\frac{71\dot{\iota}^2}{12} + \frac{\ddot{\iota}^2}{4} - \frac{7\dddot{\iota}\iota}{2} + \frac{\ddddot{\iota}\iota}{3}\right) \tag{A1}$$

and Eq. (8),

$$M^{(0)} = -\frac{d^2}{dx^2} + 1,$$

$$M^{(1)} = x\frac{d^2}{dx^2} - \frac{d}{dx}x\frac{d}{dx} - 2x,$$

$$M^{(2)} = -x^2\frac{d^2}{dx^2} + x\frac{d}{dx}x\frac{d}{dx} + 3x^2, \tag{A2}$$

where, as in the main text, dots denote dimensionless derivatives, $\dot{\iota} \equiv r_\mu d\iota/dr$, etc., and all equilibrium quantities are evaluated at $r = r_\mu$.

[1] G. Casati, B. V. Chirikov, and I. Guarneri, Phys. Rev. Lett. **54**, 1350 (1985).
[2] M. Wakatani, *Stellarator and Heliotron Devices*, No. 95 in The International Series of Monographs on Physics (Oxford University Press, New York, 1998).
[3] A. E. Lifschitz, *Magnetohydrodynamics and Spectral Theory* (Kluwer, Dordrecht, The Netherlands, 1989).
[4] G. O. Spies and J. A. Tataronis, Phys. Plasmas **10**, 413 (2003).
[5] E. Hameiri, Commun. Pure Appl. Math. **38**, 43 (1985).
[6] F. Troyon, R. Gruber, H. Saurenmann, S. Semenzato, and S. Succi, Plasma Phys. Controlled Fusion **26**, 209 (1984).
[7] J. R. Ferron *et al.*, Phys. Plasmas **7**, 1976 (2000).
[8] D. V. Anderson, W. A. Cooper, R. Gruber, S. Merazzi, and U. Schwenn, Int. J. Supercomput. Appl. **4**, 34 (1990).
[9] C. Schwab, Phys. Fluids B **5**, 3195 (1993).
[10] I. B. Bernstein, E. A. Frieman, M. D. Kruskal, and R. M. Kulsrud, Proc. R. Soc. London, Ser. A **244**, 17 (1958).
[11] R. L. Dewar and A. H. Glasser, Phys. Fluids **26**, 3038 (1983).
[12] P. Cuthbert, J. L. V. Lewandowski, H. J. Gardner, M. Persson, D. B. Singleton, R. L. Dewar, N. Nakajima, and W. A. Cooper, Phys. Plasmas **5**, 2921 (1998).
[13] M. H. Redi, J. L. Johnson, S. Klasky, J. Canik, R. L. Dewar, and W. A. Cooper, Phys. Plasmas **9**, 1990 (2002).
[14] M. C. Gutzwiller, *Chaos in Classical and Quantum Mechanics*, No. 1 in Interdisciplinary Applied Mathematics Series (Springer-Verlag, New York, 1990).
[15] H. J. Stöckmann, *Quantum Chaos: An Introduction* (Cambridge University Press, Cambridge, 1999).
[16] F. Haake, *Quantum Signatures of Chaos*, 2nd ed. (Springer-Verlag, Berlin, 2001).
[17] M. L. Mehta, *Random Matrices*, 2nd ed. (Academic Press, San Diego, 1991).
[18] R. L. Dewar, P. Cuthbert, and R. Ball, Phys. Rev. Lett. **86**, 2321 (2001).

[19] M. V. Berry and M. Tabor, Proc. R. Soc. London, Ser. A **356**, 375 (1977).
[20] B. R. Suydam, in *Proceedings of the Second International Conference on the Peaceful Uses of Atomic Energy* (United Nations, Geneva, 1958), Vol. 31, p. 157.
[21] O. K. Cheremhykh and S. M. Revenchuk, Plasma Phys. Controlled Fusion **34**, 55 (1992).
[22] H. Sugama and M. Wakatani, J. Phys. Soc. Jpn. **58**, 1128 (1989).
[23] R. L. Dewar, C. Nührenberg, and T. Tatsuno, in Proceedings of the 13th International Toki Conference, Toki, Japan, 2003 [J. Plasma Fusion Res. (to be published)].
[24] H. R. Strauss, Plasma Phys. **22**, 733 (1980).
[25] R. M. Kulsrud, Phys. Fluids **6**, 904 (1963).
[26] T. Tatsuno, M. Wakatani, and K. Ichiguchi, Nucl. Fusion **39**, 1391 (1999).
[27] B. F. McMillan, R. L. Dewar, and R. G. Storer, Plasma Phys. Controlled Fusion **46**, 1027 (2004).
[28] L. D. Landau and E. M. Lifshitz, *Quantum Mechanics (Non-relativistic Theory)*, 3rd ed. No. 3 in Course of Theoretical Physics (Pergamon, Oxford, 1991).
[29] J. W. Connor, R. J. Hastie, and J. B. Taylor, Proc. R. Soc. London, Ser. A **365**, 1 (1979).
[30] R. L. Dewar, M. S. Chance, A. H. Glasser, J. M. Greene, and E. A. Frieman, Tech. Rep. PPPL-1587, Princeton University Plasma Physics Laboratory (1979), available from National Technical Information Service, U.S. Department of Commerce, 5285 Port Royal Road, Springfield, VA 22151.
[31] I. Niven, H. S. Zuckerman, and H. L. Montgomery, *An Introduction to the Theory of Numbers*, 5th ed. (Wiley, New York, 1991).